

Performance of a Thermoelectric Device with Integrated Heat Exchangers

MATTHEW M. BARRY,^{1,2} KENECHI A. AGBIM,^{1,3}
and MINKING K. CHYU^{1,4}

1.—Department of Mechanical Engineering and Materials Science, University of Pittsburgh, Pittsburgh, PA 15261, USA. 2.—e-mail: mmb49@pitt.edu. 3.—e-mail: kaa59@pitt.edu. 4.—e-mail: mkchyu@pitt.edu

Thermoelectric devices (TEDs) convert heat directly into electrical energy, making them well suited for waste heat recovery applications. An integrated thermoelectric device (iTED) is a restructured TED that allows more heat to enter the p–n junctions, thus producing a greater power output P_o . An iTED has heat exchangers incorporated into the hot-side interconnectors with flow channels directing the working fluid through the heat exchangers. The iTED was constructed of *p*- and *n*-type bismuth-telluride semiconductors and copper interconnectors and rectangular heat exchangers. The performance of the iTED in terms of P_o , produced voltage V and current I , heat input Q_h and conversion efficiency η for various flow rates ($2190 \leq Re_{Dh} \leq 9920$), inlet temperatures ($50 \leq T_{in} (^{\circ}\text{C}) \leq 150$) and load resistances ($0 \leq R_L (\Omega) \leq 5000$) with a constant cold-side temperature ($T_c = 0^{\circ}\text{C}$) was conducted experimentally. An increase in T_{in} had a greater effect on the performance than did an increase in Re_{Dh} . A 3-fold increase in T_{in} resulted in a 3.2-, 3.1-, 9.7-, 3.5- and 2.8-fold increase in V , I , P_o , Q_h and η , respectively. For a constant T_{in} of 50°C , a 3-fold increase in Re_{Dh} from 3300 to 9920 resulted in 1.6-, 1.6-, 2.6-, 1.5- and 1.9-fold increases in V , I , P_o , Q_h and η , respectively.

Key words: Thermoelectric, flow channel, integrated heat exchanger, waste heat recovery

List of Symbols

Variables

A	Cross-sectional area, m^2
A_c	Flow cross-sectional area, m^2
A_s	Surface area, m^2
C_p	Specific heat of fluid, $\text{J kg}^{-1} \text{K}^{-1}$
D_h	Hydraulic diameter, m
I	Electric current, A
P_o	Power output, W
Q_h	Heat transfer, W
R	Electric resistance, Ohms
Re_{Dh}	Reynolds number, hydraulic diameter ($\rho_f U D_h / \mu$)
T	Temperature, $^{\circ}\text{C}$
V	Voltage, V
\dot{V}	Volumetric flow rate, L min^{-1}

Greek Symbols

α	Seebeck coefficient, V K^{-1}
η	Thermoelectric conversion efficiency, dimensionless
κ	Thermal conductivity, $\text{W m}^{-1} \text{K}^{-1}$
μ	Dynamic viscosity, N s m^{-2}
ρ	Electrical resistivity, Ohm m or density of fluid, kg m^{-3}
σ	Electrical conductivity, $\text{Ohm}^{-1} \text{m}^{-1}$

Subscripts

c	Cold side
exit	Exit
FA	Flow area
h	Hot side
in	Inlet
L	Load
max	Maximum
ohm	Ohmic
oc	Open circuit

INTRODUCTION

Since the industrial revolution, we have developed tremendous technological processes, which have included electrical energy production. Electrical energy production comes in the form of coal-, oil- and gas-fired power plants, boiling and pressurized water nuclear reactors, geothermal, hydro, and photovoltaic (PV) power generation plants and wind turbines, to name just some. It is quite evident that power production through the usage of fossil fuels has adverse effects in terms of pollution of the environment and the release of greenhouse gases (GHG). The emission of GHG, in the form of carbon dioxide, and more harmful gases like methane, chlorofluorocarbons (CFCs) and nitrous oxide^{1,2} can lead to changes in the global climate. Although the levels of GHG, in particular carbon dioxide, are not the highest they have been in the past 60 million years,³ an increase in GHG does lead to a change in the climate, as evidenced by an increase in the global temperature within the past century.

From the start of the twentieth century to 1960, the global temperature increased 0.2°C, and from 1960 to 1980, another 0.2°C.⁴ The global temperature has continued to increase at a rate of 0.15°C–0.20°C per decade since the late 1970s.⁵ Curbing the emission of greenhouse gases could mitigate the effects of global climate change,⁶ therefore much policy-making attention has been devoted to renewable and sustainable energy (RSE) production technologies.⁷ Moreover, the decarbonization of electricity generation is not enough to reduce the emission of GHG,⁸ and RSE technologies need to be developed concurrently to diversify the energy production portfolio.⁹

Although RSE production technologies like PV, concentrated solar power, geothermal, fuel cells, and biomass are promising alternatives to fossil fuel-based power generation systems, they have an inherently similar trait with the aforementioned fossil fuel systems: waste heat. Recovering any amount of waste heat and converting it into electrical energy can increase the efficiency of any cycle, device and process while mitigating potential environmental impacts. For fossil fuel-based power generation and transportation, the system can achieve more power output per unit fuel, effectively reducing GHG emissions.

Thermoelectric devices (TEDs) are well suited for waste heat recovery. These steady-state devices directly convert thermal energy into electrical energy via an applied temperature difference (Seebeck effect¹⁰). Additionally, a restructured TED can use a voltage potential to generate a temperature difference (Peltier effect¹¹). TEDs are constructed of n- and p-doped semiconductors that are connected electrically in series and operated thermally in parallel. Thermoelectric materials have a high Seebeck coefficient α , high electrical conductivity σ and low thermal conductivity κ .^{12,13} In the 1950s,

semiconductors with higher thermoelectric performance were developed, which aided in the development of devices with moderate performance.^{14,15}

The material's performance is characterized by a dimensionless figure of merit, ZT ($\sigma\alpha^2T/\kappa$), which is expressed as the ratio of the electrical conductivity σ times the square of the Seebeck coefficient α over the thermal conductivity κ times the absolute temperature T . The figure of merit depends on both materials' intrinsic properties and the hot- and cold-side temperatures, T_h and T_c , respectively.¹⁶ Efficiency enhancement of TEDs is a multi-faceted approach; material fabrication via methods of cold-^{17,18} and hot-isostatic pressing,^{19,20} nanostructuring of existing materials via mechanical alloying,^{21–27} spark plasma sintering,^{28,29} and the use of new elements¹⁶ are pursued to increase the material efficiency. To increase device performance, modeling, design and optimization of the TED system^{30–34} are pursued.

In terms of design and optimization of TED systems, cascading and segmenting of TE materials are the best methods for efficiently recovering waste heat from high-temperature sources. Cascading optimizes temperature-dependent material properties along the direction of the temperature gradient, allowing each material to operate at a temperature difference that maximizes either power output or efficiency. Fujisaka et al.³⁵ demonstrated that cascaded TEDs can increase the power output by 1.24 times and efficiency by nearly 50% as compared to conventional designs. Segmenting involves placing the high- and low-temperature materials in the waste heat up- and downstream, respectively, allowing each material to operate in the desirable temperature difference.¹⁶ Caillat et al.³⁰ demonstrated a segmented TED can achieve an efficiency of 15% over an operating temperature range of 300 K to 973 K.

Waste heat recovery applications of segmented and cascaded TEDs have already been applied to automobiles. LaGrandeur³⁶ and Crane et al.³⁷ have demonstrated that TEDs can recover exhaust gas waste heat, potentially producing enough electrical energy to aid and/or replace the secondary electro-mechanical alternator systems. The replacement of the alternator would reduce load on the engine, increasing efficiency. Crane et al.³⁴ developed a cylindrical TED comprised of segmented elements that produced a maximum power output of 608 W. They then implemented this TED concept into two passenger cars, converting exhaust gas heat into electrical power.³⁸ Furthermore, Yao et al.³⁹ discussed using TEDs in the same application using a thermal resistance network model for automobile waste heat recovery at both the radiator and the post-catalytic converter, finding that more heat energy was available within the exhaust gas. Additionally, Chau et al.⁴⁰ discussed using TEDs for both waste heat recovery and temperature control modules for hybrid vehicles.

It should be noted that TEDs are not only applicable to automotive waste heat recovery; TEDs have also been applied to hybrid photovoltaic systems.^{41–43} It has been estimated that hybrid systems could achieve nearly 23% conversion efficiency.⁴⁴

The use of typical TED structures, whether conventional, cascaded or segmented, in automotive or RSE waste heat recovery has disadvantages, such as the large thermal resistance associated with the use of ceramics and the subsequent thermal contact resistances associated with attaching the heat source and sink to said ceramics. Liang et al.³³ have shown the thermal contact resistance between the TED module and heat source and sink affects the power output of a multistage TED by reducing the temperature difference ΔT the TE material realizes. To address the current issue of a large thermal resistance between the source and sink when applying conventional TEDs to waste heat recovery applications, the authors^{45–51} have proposed an integrated thermoelectric device (iTED).

An iTED is a reconfigured conventional TED where the hot-side heat exchanger is directly incorporated into the hot-side interconnector. The hot-side heat exchanger is not electrically insulated from the TE materials, allowing the device to operate electrically in series and thermally in parallel. The working fluid is then directed through the hot-side heat exchanger via flow channels, which prevent the working fluid from entering the cavity between the thermoelectric legs. This configuration eliminates the need for an electrically insulating and low thermal conductivity ceramic plate between the hot-side heat exchanger and interconnector. For a given set of operating conditions, the iTED has increased performance in terms of power output as compared to a conventional TED due to the decreased thermal resistance between the heat source and sink; this reduction increases the temperature difference across the thermoelectric elements, thereby increasing the power output. This study presents the experimental investigations on the performance of a single-stage iTED comprised of *n*- and *p*-type bismuth-telluride semiconductors applied to low-grade waste heat recovery under various inlet flow conditions. The influence of inlet flow rate and temperature and load resistance on the iTED's performance in terms of thermoelectric characteristics are investigated.

MATERIALS AND METHODS

An integrated thermoelectric device (iTED) was made with bulk *n*-type 75% Bi₂Te₃-25% Bi₂Se₃ and *p*-type 25% Bi₂Te₃-75% Sb₂Te₃ (1.75% excess Se) bismuth-telluride semiconductors. The *n*- and *p*-type bismuth-telluride square cuboids were chemically bonded onto the top and bottom surfaces of medium-phosphorus nickel-plated oxygen-free high thermal conductivity (OFHC) copper heat

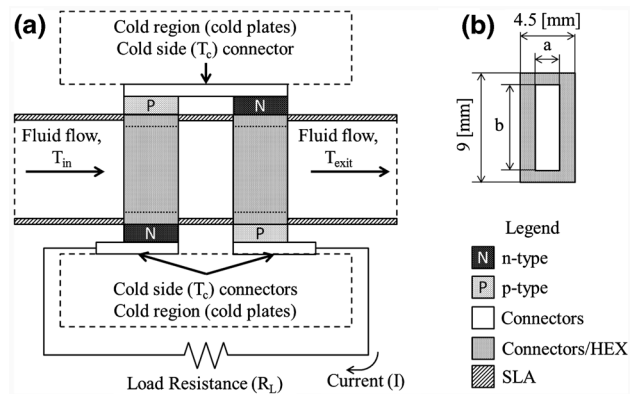


Fig. 1. Schematics of (a) an integrated thermoelectric device and (b) cross-sectional view of the flow channel configuration; $a = 2$ mm and $b = 7.1$ mm.

exchangers using a silver-filled epoxy ($\rho \leq 0.4$ m Ω -cm, $\kappa = 8$ W m⁻¹ K⁻¹). The hot-side heat exchangers had internal rectangular flow channels and were also the hot-side interconnectors for the *p*-*n* junctions. This arrangement allowed the *n*- and *p*-type thermoelectric materials to be in direct contact, both thermally and electrically, to the hot-side heat exchanger, thereby eliminating the need for an electrical insulator, like ceramics, as seen in conventional TED designs. The iTED operates thermally in parallel and electrically in series like a conventional TED.

The *p*-*n* junctions not established via the internal heat exchangers were established through medium-phosphorus nickel-plated OFHC interconnectors, which were in contact with, but electrically isolated from, a cold reservoir of temperature T_c and acted as terminals when the device was connected to external loads of resistance R_L . Figure 1a depicts an iTED module. The geometry of a leg (single *p*-*n* junction) within an iTED module is as follows: the *p*- and *n*-type thermoelectric materials had a cross-sectional area of 25 mm² (5 mm by 5 mm) and a thickness of 1 mm; the heat exchanger had a cross-sectional area of 25 mm² (5 mm by 5 mm) and height of 10 mm; the interconnector had a width of 5 mm, length of 15 mm and height of 1 mm.

Inlet flow was directed from the source to the first heat exchanger, between the first and second heat exchangers and then away from the module through electrically insulated flow channels. The flow channels were constructed of Somos[®] NanoTool resin and printed using stereolithography by Fineline[™] (Raleigh, NC, USA). The inlet and exit channels had sufficient length such that fully developed flow was established before entering the first heat exchanger and before exiting the iTED. The length of the intermediate channel was 5 mm. The internal width and height of the inlet, intermediate and exit channel was 4.5 mm by 9 mm. The flow cross-sectional area A_c of the hot-side heat exchanger was 14.2 mm² and the surface area A was 90.7 mm².

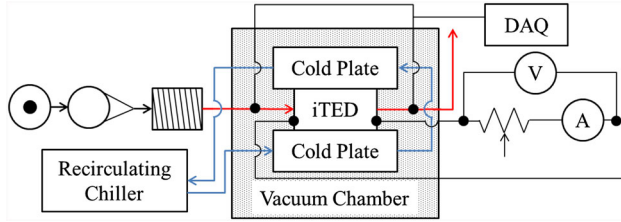


Fig. 2. Schematic of test set-up. Compressed air is passed through a rotameter and coil heater before entering the iTED module. A voltmeter is used to measure the voltage drop across the ammeter and resistance simulator (potentiometer).

The ratio of A to A_c of the hot-side heat exchanger was $\phi_{FA} = 6.4$. Figure 1b depicts the heat exchanger geometry that was exposed to the flow.

EXPERIMENTAL

Figure 2 illustrates the schematic of the experimental setup. The iTED was placed in a vacuum chamber with a working vacuum of 27.5 inHg to minimize convection from the external surfaces. Hot air was passed through the iTED via the inlet channel with flow rates (\dot{V}) varying from 100 L min⁻¹ to 200 L min⁻¹ and temperatures between 50°C and 150°C. Compressed air was passed through a Dwyer VFB-55-SSV rotameter and a coil-wrapped heater before entering the iTED. The inlet and exit temperatures (T_{in} and T_{exit}) of the air was measured with high-temperature K-type thermocouples. All thermocouple voltages were measured using a National Instruments Data Acquisition system (NiDAQ) with a built-in reference temperature and analyzed using National Instruments VI-Logger software.

The heat Q_h added to the iTED is expressed by Eq. 1. Q_h was calculated via the volumetric flow rate of the fluid \dot{V} , the temperature-dependent density ρ and specific heat C_p , which were evaluated at the average temperature of the fluid flow (i.e. the average of the inlet and exit temperatures, T_{in} and T_{exit}) and the temperature difference between the inlet and exit fluid flow, such that

$$Q_h = \dot{V} \rho C_p (T_{in} - T_{exit}). \quad (1)$$

To simulate a cold-side reservoir, the top and bottom surfaces of the iTED were placed in contact with electrically insulated cold plates. A 50/50 mixture of water and ethylene glycol was passed through the cold plates using a recirculating chiller. The temperatures of the cold plates were kept constant at $T_c = 0^\circ\text{C}$.

The iTED was connected electrically in series to an Agilent U3606A ammeter and an IET Labs RS-RTD resistance simulator which represented load circuitry of resistance R_L . The U3606A was used to measure the produced current I . An Agilent U34401A multimeter was used to measure the voltage V produced by the iTED, which is the summation of the Ohmic V_{ohm} and Seebeck V_{oc}

voltages. The uncertainties associated with the voltage and current measurements are 0.025%. The resistance simulator's load resistance R_L was adjusted between 0.01 ohms and 5000 ohms and the power output of the iTED was calculated via the second and third expressions of Eq. 2, which is expressed as

$$P_o = IV = I^2 R_L = \frac{\alpha^2 R_L}{(R_L + R_{in})^2} \Delta T^2. \quad (2)$$

Evaluating the second and third expressions of Eq. 2 yields the same result within error of the measurement system. The term α of the fourth expression is the summation of the absolute values of n - and p -type Seebeck coefficients, R_{in} is the internal resistance of the iTED and ΔT is the temperature difference across the p-n junctions. The fourth expression of Eq. 2 is provided only to illustrate the effect of R_L and ΔT on P_o and was not evaluated to determine P_o . The efficiency of the iTED was calculated using the power output and heat input, expressed as

$$\eta = \frac{P_o}{Q_h}. \quad (3)$$

A FLIR® SC-325 thermal camera was used to image the surface of the iTED and determine the temperature difference ΔT across the thermoelectric elements. The iTED was painted matte black and the camera was calibrated to thermocouple measurements at 25°C and 150°C. The thermal images were evaluated using FLIR® ExaminIR™ software. Each test was conducted three times to determine the average temperatures of the working fluid and the thermoelectric characteristics V , I , P_o , Q_h and η , as well as ΔT .

RESULTS AND DISCUSSION

The thermoelectric performance of an integrated thermoelectric device with a rectangular flow channel in terms of produced electric current I and voltage V , calculated power output P_o and thermal conversion efficiency η under various flow conditions ($2190 \leq Re_{Dh} \leq 9920$, $50 \leq T_{in} (^{\circ}\text{C}) \leq 150$) and load resistances ($0 \leq R_L (\Omega) \leq 5000$) has been experimentally investigated. The effect of inlet temperature, flow rate, as expressed by the Reynolds number, and load resistance are presented.

Effect of Inlet Temperature

Figure 3 illustrates the electrical characteristics for an integrated thermoelectric device under various fluid inlet temperatures and Reynolds numbers ($50 \leq T_{in} (^{\circ}\text{C}) \leq 150$, $2190 \leq Re_{Dh} \leq 3300$). The produced voltage V is the summation of the V_{ohm} and V_{oc} voltages. V obeys Ohm's law such that it is equal to the produced current I time the resistance R , which is the summation of the load R_L and internal

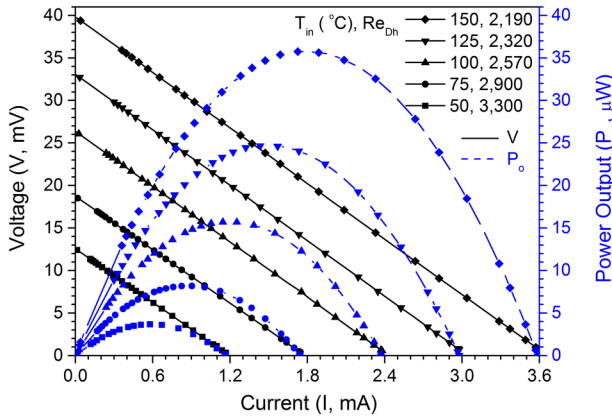


Fig. 3. Voltage V , current I and power output P_o of an iTED with various inlet temperatures T_{in} and Reynolds numbers Re_{Dh} with a cold-side temperature of 0°C .

R_{in} resistance. The increase in voltage scales linearly with an increase in fluid inlet temperature T_{in} . For instance, as T_{in} increases from 50°C to 75°C and 125°C to 150°C (1.5- and 1.2-fold increase), the maximum voltage increases from 12.52 mV to 18.66 mV and 33.00 mV to 39.72 mV (1.5- and 1.2-fold increase). Likewise, the I produced follows the same linear trend with an increase in T_{in} , such that as a 3-fold increase in T_{in} resulted in an increase in the maximum I value by 3.1-fold, as evidenced by Fig. 3 and Fig. 4. The P_o increases non-linearly with an increase in T_{in} ; as T_{in} is increased 1.5-, 2-, 2.5- and 3-fold for the 3300 to 2190 Re_{Dh} cases (Fig. 3), the maximum power output increased 2.2-, 4.3-, 6.7- and 9.7-fold, respectively.

Figure 5 illustrates the effects of T_{in} on the maximum power output $P_{o,max}$ and maximum produced voltage V_{max} . Increasing T_{in} drastically increases $P_{o,max}$ and V_{max} values. For roughly the same Re_{Dh} values (3300 and 2190), a 3-fold increase in T_{in} (50°C to 150°C) results in a 9.7- and 3.2-fold increase in $P_{o,max}$ and V_{max} values, respectively. $P_{o,max}$ is proportional to ΔT^2 as seen by the fourth expression of Eq. 2. By increasing T_{in} from 50°C to 150°C , the temperature difference across the thermoelectric legs ΔT , as measured by the thermal camera, increased from 19.0°C to 58.4°C , as illustrated in Fig. 6. The 3-fold increase in T_{in} resulted in a 3.1-fold increase in ΔT across the TE material, which corresponds very closely to the 9.7-fold increase in $P_{o,max}$ and is within error of the measurement system.

Figure 7 illustrates that increasing T_{in} increases Q_h and η . The heat input Q_h increases more than η with the same increase in T_{in} such that a 1.5-, 2-, 2.5 and 3-fold increase in T_{in} results in a 1.8-, 2.2-, 2.7- and 3.5-fold increase in Q_h and a 1.2-, 1.9-, 2.4- and 2.8-fold increase in η . As T_{in} increases from 50°C to 150°C , the density of the working fluid decreases from 1.097 kg m^{-3} to 0.835 kg m^{-3} and the dynamic

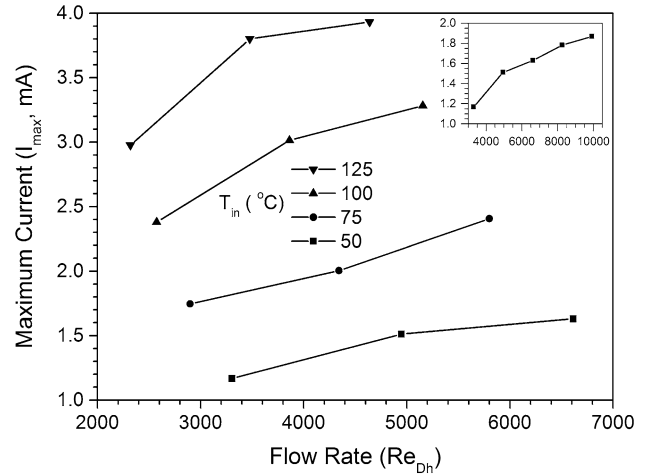


Fig. 4. Effect of increasing flow rate Re_{Dh} and inlet temperature T_{in} on the maximum produced current I_{max} at $R_L=0\ \Omega$. Inset shows I_{max} versus Re_{Dh} for $T_{in}=50^\circ\text{C}$ series with high Re_{Dh} .

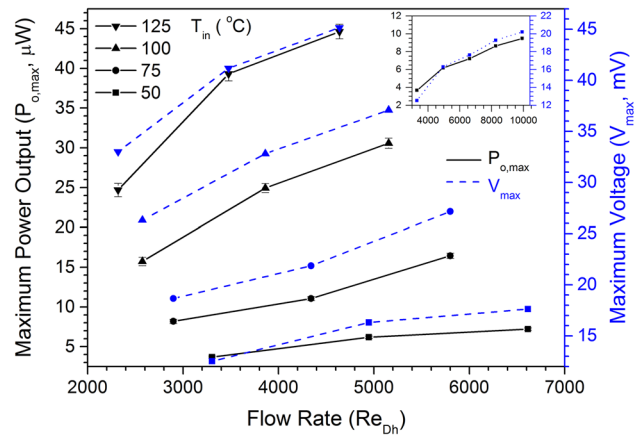


Fig. 5. Effect of increasing flow rate Re_{Dh} and inlet temperature T_{in} on maximum power output $P_{o,max}$ and maximum voltage V_{max} predictions. Inset shows $P_{o,max}$ and V_{max} versus Re_{Dh} for $T_{in}=50^\circ\text{C}$ series with high Re_{Dh} .

viscosity increases from $1.760 \cdot 10^{-5}$ to $4.623 \cdot 10^{-5}\text{ kg m}^{-1}\text{s}^{-1}$, resulting in a decreasing Reynolds number for the same flow area (i.e. from 3300 to 2190). With a decreasing Reynolds number comes a decrease in the convective heat transfer coefficient h , which would decrease Q_h for a given T_{in} . Although Re_{Dh} decreases 33.6% with a 3-fold increase in T_{in} , these Re_{Dh} values lie within the transition region between laminar and turbulent flow and the effect of decreasing Re_{Dh} on h and subsequent Q_h values are unclear and non-linear. Despite the potential decrease in h with an increase in T_{in} , ΔT increases linearly which results in a non-linear increase in P_o . Furthermore, Q_h increases with T_{in}

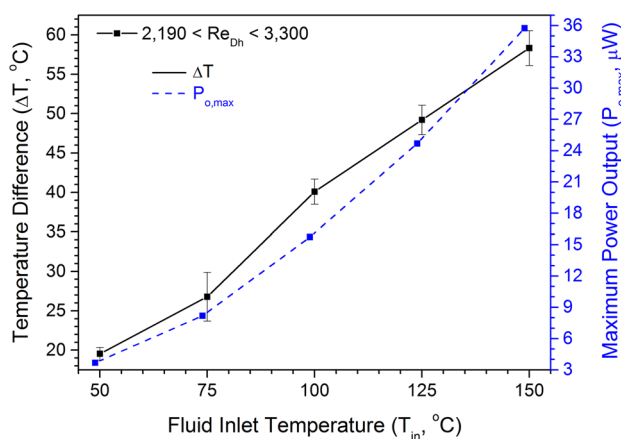


Fig. 6. Effect of inlet temperature T_{in} on temperature difference ΔT across TE materials and maximum power output $P_{o,max}$ predictions.

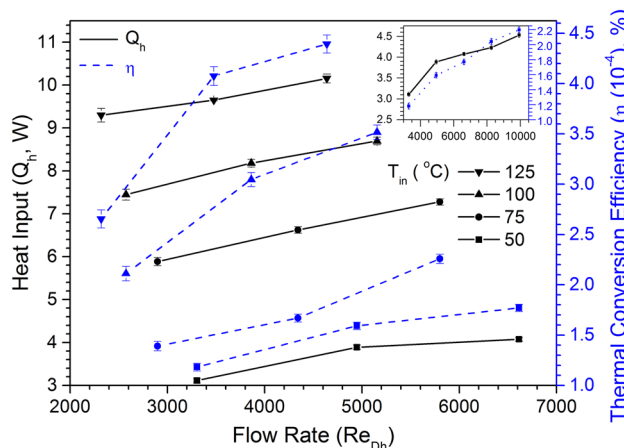


Fig. 7. Effect of increasing flow rate Re_{Dh} and inlet temperature T_{in} on heat input Q_h and thermal conversion efficiency η predictions. Inset shows Q_h and η versus Re_{Dh} for $T_{in}=50^\circ\text{C}$ series with high Re_{Dh} .

and more substantially than the increase in P_o , resulting in a non-linear increase in η .

Effect of Reynolds Number Re_{Dh}

The effect of flow rate on the maximum produced current I_{max} (evaluated at $R_L=0 \Omega$) is illustrated in Fig. 4 with the high Re_{Dh} cases depicted in the inset. For an inlet temperature of 50°C , a 1.5-, 2-, 2.5- and 3-fold increase in Re_{Dh} results in a 1.3-, 1.4-, 1.5- and 1.6-fold increase in I_{max} . Figure 5 illustrates the effects of Re_{Dh} on the V_{max} and $P_{o,max}$ for various inlet temperatures. It is evident that an increase in Re_{Dh} marginally increases the maximum power output. With T_{in} invariant at 50°C , a 2- and 3-fold increase in the Re_{Dh} values from 3300 to 6610 and 9920 results in a 2.0- and 2.6-fold increase in $P_{o,max}$, a 1.4- and 1.6-fold increase in V_{max} , and a 1.4- and

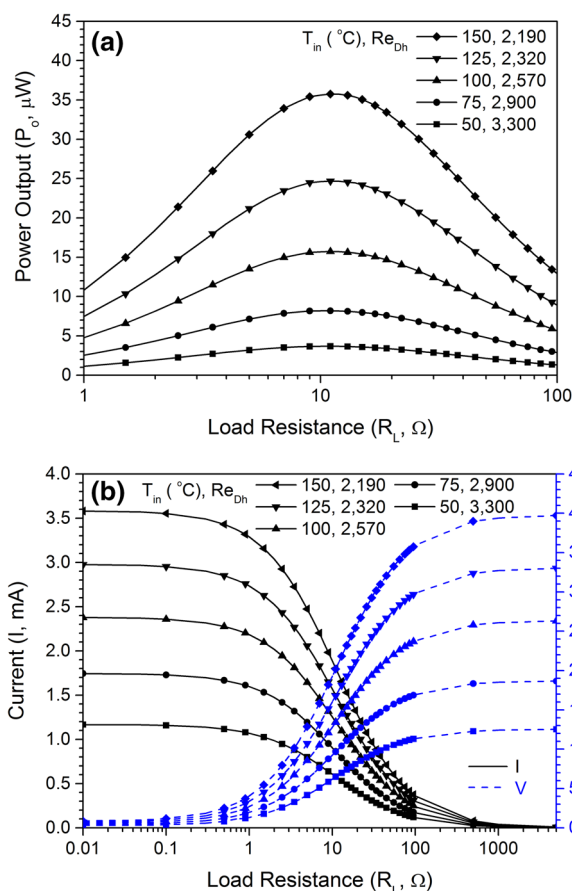


Fig. 8. The effect of load resistance R_L on (a) power output P_o and (b) produced current I and voltage V for various inlet temperatures T_{in} and flow rates Re_{Dh} .

1.6-fold increase in I_{max} . This trend is seen in all cases with different inlet temperatures.

Figure 7 shows how an increase in Re_{Dh} causes an increase in Q_h and η . As the flow departs the transition region and becomes turbulent, i.e. an increase in Re_{Dh} , the convective heat transfer coefficient h increases. A rise in h increases Q_h and thus produces a larger ΔT across the TE elements and subsequently a larger P_o . For instance, given $T_{in}=50^\circ\text{C}$, a 2- and 3-fold increase in Re_{Dh} from 3300 to 6610 and 9920 resulted in a 1.3- and 1.5-fold increase Q_h and a 2.0- and 2.6-fold increase in $P_{o,max}$, yielding a 1.5 and 1.9-fold increase in η .

However, increasing Re_{Dh} does not have as substantial an effect on the ΔT imposed upon the TE elements as does increasing T_{in} . As Re_{Dh} increased from 3300 to 9920 (3-fold) at a constant inlet temperature of 50°C , ΔT across the TE elements increased marginally from 19.0°C to 28.9°C , yielding a 1.5-fold increase; in comparison, ΔT increased from 19.0°C to 58.4°C (3.1-fold) as T_{in} increased 3-fold from 50°C to 150°C .

Effect of Load Resistance

For an iTED with inlet fluid temperatures of 50°C to 150°C and corresponding Re_{Dh} varying from 3300 to 2190, Fig. 8a illustrates the effect of R_L on the P_o and Fig. 8b of R_L on I and V . From Fig. 8a, $P_{o,max}$ is produced when the R_L is equal to the R_{in} . The measured internal device resistance was 0.46 Ω at ambient, non-operating conditions, however, the system resistance including cables and connections resulted in a total system resistance of approximately 10 Ω during operating conditions. As T_{in} increases, there is a slight increase in R_{in} of the device as seen by a shift in the maxima of the curves in Fig. 8a, thus the optimum load resistance increases.

It is evident from Fig. 8b that the produced I decays while the produced V increases as R_L increases. As the total resistance increases (sum of R_{in} and R_L), V must increase and I must decrease as dictated by Ohm's law. The P_o as evaluated by the second expression of Eq. 2 reaches the maximum $P_{o,max}$ when the load resistance is equal to the internal resistance, and is found where the curves depicting current and voltage intersect. These two methods, that of the maxima as illustrated in Fig. 8a (I^2R_L) and of the intersection of the I and V curves as in Fig. 8b (IV), yield concurrent optimum R_L and $P_{o,max}$ values. Irrespective of Re_{Dh} and T_{in} , the P_o and produced I and V trends follow the same behavior with a change in R_L .

CONCLUSIONS

An integrated thermoelectric device (iTED) is a restructured TED in which the hot-side heat exchanger is integrated into the hot-side interconnector. The working fluid is then directed through the integrated heat exchanger via flow channels. This configuration reduces the thermal resistance between the waste heat source and sink, allowing for greater heat input and power output. The effects of inlet fluid temperature ($50 \leq T_{in} (^{\circ}C) \leq 150$) and flow rate ($2190 \leq Re_{Dh} \leq 9920$) and load resistance ($0 \leq R_L (\Omega) \leq 5000$) on the performance of an iTED in terms of produced current I and voltage V , power output P_o , heat input Q_h and conversion efficiency η have been studied.

It was found that T_{in} had a more substantial effect on the performance of an iTED than did Re_{Dh} . The P_o increases non-linearly with T_{in} whereas I , V , Q_h and η increase near-linearly in T_{in} . A 3-fold increase in T_{in} resulted in a 3.1-fold increase in ΔT across the TE material, which resulted in a 9.7-fold increase in $P_{o,max}$. For the same increase in T_{in} , the values of I_{max} , V_{max} , Q_h and η increased 3.1-, 3.2-, 3.5- and 2.8-fold, which is attributed to the linear increase of ΔT across the TE material with T_{in} .

Increasing Re_{Dh} while T_{in} was fixed, the V , I , $P_{o,max}$, Q_h and η values did not increase as drastically compared to an increase in T_{in} . For a constant $T_{in}=50^{\circ}C$, a 3-fold increase in Re_{Dh} resulted in a 1.6-

1.6-, 2.6-, 1.5- and 1.9-fold increase in V_{max} , I_{max} , $P_{o,max}$, Q_h and η , respectively. Increasing Re_{Dh} increased the convective heat transfer coefficient h , which increases the amount of heat delivered to the heat exchangers. However, the non-linear increase in h and subsequent Q_h did not increase the ΔT across the thermoelectric elements as drastically as an increase in T_{in} , thus the performance did not increase as greatly as compared to an increase in T_{in} . For instance, with a constant $T_{in}=50^{\circ}C$, a 3-fold increase in Re_{Dh} resulted in a 1.5-fold increase in ΔT .

Increasing the load resistance R_L increases the produced V and decreases the produced I . Additionally, increasing R_L up to the value of the internal resistance R_{in} increases P_o to the maximum $P_{o,max}$; an increment in R_L beyond R_{in} then decreases P_o .

ACKNOWLEDGEMENTS

The authors would like to thank Andrew Holmes of the Swanson Center for Product Innovation at the University of Pittsburgh for his assistance in fabricating the iTED modules. The authors would also like to thank Professor Emad Mirmotahari from Duquesne University for his assistance in editing this manuscript.

REFERENCES

1. D.A. Lashof and D.R. Ahuja, *Relative Contributions of Greenhouse Gas Emissions to Global Warming* (Nature Publishing Group, New York, 1990), pp. 529–531.
2. J. Hansen, M. Sato, P. Kharecha, G. Russell, D.W. Lea, and M. Siddall, *Philos. Trans. R. Soc. Lond. A* 365, 1925 (2007).
3. P.N. Pearson and M.R. Palmer, *Nature* 406, 695 (2000).
4. J. Hansen, D. Johnson, A. Lacis, S. Lebedeff, P. Lee, D. Rind, and G. Russell, *Science* 213, 957 (1981).
5. J. Hansen, R. Ruedy, M. Sato, and K. Lo, *Rev. Geophys.* 48, RG4004 (2010).
6. M. Meinshausen, N. Meinshausen, W. Hare, S.C. Raper, K. Frieler, R. Knutti, D.J. Frame, and M.R. Allen, *Nature* 458, 1158 (2009).
7. Climate Change Mitigation, IPCC special report on renewable energy sources and climate change mitigation.
8. J.H. Williams, A. DeBenedictis, R. Ghanadan, A. Mahone, J. Moore, W.R. Morrow, S. Price, and M.S. Torn, *Science* 335, 53 (2012).
9. N. Panwar, S. Kaushik, and S. Kothari, *Renew. Sustain. Energy Rev.* 15, 1513 (2011).
10. T.J. Seebeck, *Ann. Phys.* 82, 253 (1826).
11. J. Peltier, *Ann. Chem.* LVI, 371 (1834).
12. E. Altenkirch, *Phys. Z.* 10, 560 (1909).
13. E. Altenkirch, *Phys. Z.* 12, 920 (1911).
14. A.F. Ioffe, *Semiconductor Thermoelements and Thermoelectric Cooling* (Infosearch, London, 1957).
15. A.F. Ioffe, *Sci. Am.* 199, 31 (1958).
16. D.M. Rowe (ed.), *Thermoelectrics Handbook Macro to Nano* (CRC Press, Taylor & Francis Group, Boca Raton, 2006).
17. J. Navratil, Z. Starý, and T. Plechacek, *Mater. Res. Bull.* 31, 1559 (1996).
18. C.-N. Liao, L.-C. Wu, and J.-S. Lee, *J. Alloys Compd.* 490, 468 (2010).
19. J. Shen, Z. Yin, S. Yang, C. Yu, T. Zhu, and X. Zhao, *J. Electron. Mater.* 40, 1095 (2011).
20. X. Ji, X. Zhao, Y. Zhang, B. Lu, and H. Ni, *J. Alloys Compd.* 387, 282 (2005).

21. F. Yu, J. Zhang, D. Yu, J. He, Z. Liu, B. Xu, and Y. Tian, *J. Appl. Phys.* 105, 094303 (2009).
22. M.-P. Lu, and C.-N. Liao, *J. Alloys Compd.* 571, 178 (2013).
23. J.R. Sootsman, D.K. Chung, and M.G. Kanatzidis, *Angew. Chem. Int. Ed. Engl.* 48, 8616 (2009).
24. T.M. Tritt, *Annu. Rev. Mater. Res.* 41, 433 (2011).
25. K. Biswas, J. He, I.D. Blum, C. Wu, T.P. Hogan, D.N. Seidman, V.P. Dravid, and M.G. Kanatzidis, *Nature* 489, 414 (2012).
26. B. Poudel, Q. Hao, Y. Ma, Y. Lan, A. Minnich, B. Yu, X. Yan, D. Wang, A. Muto, D. Vashaee, X. Chen, J. Liu, M.S. Dresselhaus, G. Chen, and Z. Ren, *Science* 320, 634 (2008).
27. J. Yang, X. Fan, R. Chen, W. Zhu, S. Bao, and X. Duan, *J. Alloys Compd.* 416, 270 (2006).
28. J. Hassel and J. Tervo, *J. Electron. Mater.* 42, 1745 (2013).
29. J. Virta and J. Tervo, Experimenting with hot isostatically pressed (HIP) nano grained bismuth-telluride-based alloys, in *9th European Conference on Thermoelectrics: ECT2011*, vol. 1449 (AIP Publishing, New York), pp. 544–547 (2012).
30. T. Caillat, J. P. Fleurial, G. J. Snyder, A. Zoltan, D. Zoltan, and A. Borshchevsky, Development of a high efficiency thermoelectric uncouple for power generation applications, *Proceedings of the XVIII International Conference on Thermoelectrics*, (Baltimore, 1999).
31. H. Kaibe, I. Aoyama, M. Mukoujima, T. Kanda, S. Fujimoto, T. Kurosawa, H. Ishimabushi, K. Ishida, L. Rauscher, Y. Hata, and S. Sano, Development of thermoelectric generating stacked modules aiming for 15% of conversion efficiency, in *International Conference on Thermoelectrics, IEEE*, pp. 242–247 (2005).
32. M. Hodes, *IEEE Trans. Compon. Packag. Technol.* 33, 307 (2010).
33. G. Liang, J. Zhou, and X. Huang, *Appl. Energy* 88, 5193 (2011).
34. D. Crane, C. Koripella, and V. Jovovic, *J. Electron. Mater.* 41, 1524 (2012).
35. T. Fujisaka, H. Sui, and R.O. Suzuki, *J. Electron. Mater.* 42, 1688 (2013).
36. J. LaGrandeur, D. Crane, S. Hung, B. Mazar, and A. Eder, Automotive waste heat conversion to electric power using skutterudite, TAGS, PbTe and BiTe, *ICT06, 25th International Conference on Thermoelectrics*, pp. 343–348 (2006).
37. D. Crane and J. LaGrandeur, *J. Electron. Mater.* 39, 2142 (2010).
38. D. Crane, J. LaGrandeur, V. Jovovic, M. Ranalli, M. Addinger, E. Poliquin, J. Dean, D. Kossakovski, B. Mazar, and C. Maranville, *J. Electron. Mater.* 42, 1582 (2012).
39. D.-J. Yao, K.-J. Yeh, C.-T. Hsu, B.-M. Yu, and J.-S. Lee, *IEEE Nanotechnol. Mag.* 3, 28 (2009).
40. K. Chau and C. Chan, *Proc. IEEE* 95, 821 (2007).
41. D. Yang and H. Yin, *IEEE Trans. Energy Convers.* 26, 662 (2011).
42. N. Wang, L. Han, H. He, N.-H. Park, and K. Koumoto, *Energy Environ. Sci.* 4, 3676 (2011).
43. G. Rockendorf, R. Sillmann, L. Podlowski, and B. Litzenburger, *Solar Energy* 67, 227 (1999).
44. W. Sark, *Appl. Energy* 88, 2785 (2011).
45. M. Chyu, B. Reddy, M. Barry, and J. Li, Enhanced heat transfer characteristics and performance of composite thermoelectric devices, *International Conference on Advanced Computational Methods and Experiments in Heat Transfer XII*, vol. 35, pp. 13–24 (2012).
46. B.V.K. Reddy, M. Barry, J. Li, and M.K. Chyu, *Energy Proc.* 14, 2088 (2012).
47. B.V.K. Reddy, M. Barry, J. Li, and M.K. Chyu, Comprehensive numerical modeling of thermoelectric devices applied to automotive exhaust gas waste-heat recovery, in *ASME 2013 Heat Transfer Summer Conference collocated with the ASME 2013, 7th International Conference on Energy Sustainability and the ASME 2013, 11th International Conference on Fuel Cell Science, Engineering and Technology*, American Society of Mechanical Engineers (2013).
48. B.V.K. Reddy, M. Barry, J. Li, and M.K. Chyu, *Front. Heat Mass Transf.* 4, 023001 (2013).
49. B.V.K. Reddy, M. Barry, J. Li, and M.K. Chyu, *J. Heat Transf.* 135, 031706 (2013).
50. B.V.K. Reddy, M. Barry, J. Li, and M.K. Chyu, Thermoelectric-hydraulic performance of a multistage integrated thermoelectric power generator. *Energy Convers. Manag.* 77, 458 (2014).
51. B.V.K. Reddy, M. Barry, J. Li, and M.K. Chyu, *Numer. Heat Transf. Part A* 62, 933 (2012).